DTU Library

Chance-Constrained Optimal Configuration of BESS Considering Uncertain Power Fluctuation and Frequency Deviation under Contingency

Cao, Yongji; Wu, Qiuwei; Zhang, Hengxu; Li, Changgang; Zhang, Xuan

Published in:
IEEE Transactions on Sustainable Energy

Link to article, DOI:
10.1109/TSTE.2022.3192087

Publication date:
2022

Document Version
Peer reviewed version

Chance-Constrained Optimal Configuration of BESS Considering Uncertain Power Fluctuation and Frequency Deviation under Contingency

Yongji Cao, *Member, IEEE*, Qiuwei Wu, *Senior Member, IEEE*, Hengxu Zhang, *Member, IEEE*, Changgang Li, *Member*, *IEEE*, Xuan Zhang, *Senior Member, IEEE*

***Abstract*—With the accelerating integration of variable renewable energies (VREs), power systems become more vulnerable to active power disturbances, and more drastic frequency dynamics emerge. The battery energy storage system (BESS) is able to handle the uncertainties of VREs, and the decreasing system inertia and frequency regulation capability. This paper proposes a chance-constrained optimal configuration scheme for the BESS to maintain both the uncertain power fluctuations and frequency deviation within predefined limits. First, the required frequency regulation capability of the BESS constrained by the maximum transient frequency deviation (MTFD) and quasi-steady-state frequency deviation (QSSFD) is estimated. Then, the kernel density estimation method is utilized to model the net power fluctuations of VREs and load. A multi-objective chance-constrained programming model accounting for the life cycle cost, energy arbitrage, uncertain power fluctuation, MTFD, and QSSFD is established to optimize the capacity of the BESS. Furthermore, the Bernstein approximation is utilized to process the chance constraint, and transform the optimization model into a deterministic form. Based on the linear weighted method and Benders decomposition, the optimization model is solved through alternating iteration. Case studies were conducted to validate the proposed scheme, showing superior performance in smoothing uncertain power fluctuations, and reducing frequency deviation under contingencies.**

***Index Terms*—Battery energy storage system, chance-constrained optimization, frequency regulation, frequency stability, system frequency response model**

I. Introduction

THE integration of variable renewable energies (VREs), e.g., wind and photovoltaic (PV) power, plays a significant role in energy transformation and emission reduction, and grows very fast [1]. However, with the increasing proportion of VREs in the energy mix, power systems are faced with the problems of uncertain power fluctuations and frequency stability. Due to the inherent intermittent and non-dispatchable characteristics, additional uncertainties are introduced by VREs to the supply side, and aggravates the power fluctuation in normal operation [2], [3]. Besides, VERs are integrated to power systems through power electronic converters, and provide limited inertia response and frequency regulation capability [4], [5]. The replacement of synchronous generators decreases the system inertia and weakens frequency regulation capability of power systems, which deteriorates the frequency dynamic response under contingencies. In order to improve the accommodation of VREs, there is an urgent need for additional controllable resource to deal with the problems of uncertain power fluctuations and frequency stability.

The battery energy storage system (BESS) is a kind of flexible controllable resource for various applications in power systems [6]-[8]. With adjustable and bi-directional output power, the BESS is promising to assist synchronous generators for power balance under both steady-state operation and contingencies [9]. More specially, the BESS can track the power variation of VREs to relief the impacts of uncertainties on power systems. In addition, the BESS is able to compensate power imbalance and arrest frequency excursion when the power system is subject to severe disturbances.

Extensive research has been carried out on the planning of the BESS [10]-[13], and the coordinated configuration of the BESS and VREs [14]-[16]. An optimization model of the BESS for microgrid applications was formulated, where the non-linear relationship of the depth of discharge and lifespan is approximated by a piecewise linearization method [10]. With the consideration of performance degrading, the site and size of the BESS was optimized by the Branch-and-Bound algorithm and convex programming [11]. A multi-objective bi-level optimization model was presented for the planning of the BESS to improve operation benefits and reduce the curtailment of wind energy [12]. The supervised learning algorithm was used to substitute the power flow constraints, and assist the planning of the BESS [13]. In addition, a scenario-based stochastic planning method was proposed for the active distribution network to determine the optimal configuration of wind turbine generators (WTGs), PV panels, and BESSs [14]. Using a two-stage framework, the coordinated planning of distributed WTGs and BESSs was conducted to manage intermittency and improve cost efficiency [15]. A fuzzy demand-side management method

This work was jointly supported by National Natural Science Foundation of China 52177096 and Shandong Provincial Natural Science Foundation ZR2021QE133. *(Corresponding author: Qiuwei Wu)*

Yongji Cao is with the Center for Electric Power and Energy, Department of Electrical Engineering, Technical University of Denmark, Kgs. Lyngby 2800, Denmark (e-mail: caoyong@dtu.dk).

Qiuwei Wu and Xuan Zhang are with Tsinghua-Berkeley Shenzhen Institute, Tsinghua Shenzhen International Graduate School, Tsinghua University, Shenzhen 518055, China (e-mail: qiuwu@sz.tsinghua.edu.cn, xuanzhang@sz.tsinghua.edu.cn).

Hengxu Zhang and Changgang Li are with the Key Laboratory of Power System Intelligent Dispatch and Control of the Ministry of Education, Shandong University, Jinan 250061, China (e-mail: zhanghx@sdu.edu.cn; lichgang@sdu.edu.cn)

considering the state of charge (SOC) and day-ahead forecasting errors was designed, on which the capacities of the BESS and VREs were optimized [16].

Moreover, the frequency regulation has been considered in the dispatching and control strategies of the BESS [17]-[22]. The biding and SOC recovery methods were proposed for the BESS to provide frequency regulation [17]. Based on the reformulation-linearization technique, a bi-level non-convex optimization model was built and solved for the participation of the BESS in energy and frequency regulation service markets [18]. According to the forecasts of PV power, a day-ahead and intra-day scheduling strategy of the BESS was presented to guarantee reliable frequency regulation capability [19]. Taking into account the range of SOC, a PI-lead and lead-lag controller was proposed for the BESS to stabilize transient voltage and frequency [20]. Besides, the dual extended Kalman filter was utilized to estimate the states of the BESS, on which the virtual inertia and droop parameters can be adjusted for power system stability [21]. With the use of a multi-agent system framework, a distributed control method was proposed to coordinate multiple BESSs for frequency regulation [22].

The improvement of dispatching and control strategies of the BESS is useful to deal with the problems incurred by VREs. However, the upper bound of the response capability of the BESS is determined by the configuration scheme. Therefore, both the uncertainties and frequency regulation should be considered in the planning of the BESS for the further accommodation of VREs. The uncertain power fluctuation can be smoothed in the steady-state operation, where the output power of the BESS is dispatched. There is a conflict between the operation profits and fluctuation smoothing. Besides, the time step of BESS dispatching is about 15 min~1 h. But frequency dynamic response is an electromechanical transient process, of which the time duration is about 10~30 s. The two active power balance problems take place in different time scales. Additionally, the allocation of power and energy between the fluctuation smoothing and frequency regulation also are contradictory. How to optimize the size of the BESS considering the contradictory and multi-time-scale factors is a challenge.

There are extensive studies using the BESS to smooth power fluctuation [10]-[16], and frequency regulation [17]-[22]. However, the power smoothing in the normal operating state, and frequency regulation during the transient process were usually considered independently. For the planning of the BESS, extensive studies have considered the power smoothing [10]-[16], but limited studies have taken into account the frequency regulation under contingencies [23], [24]. Besides, these BESS planning schemes do not consider the above two issues simultaneously. In our earlier work, the BESS and supercapacitor were optimized to improve the power smoothing and frequency regulation simultaneously [25]. However, there are still two research gaps not filled. First, the uncertainty of the VREs was not considered. Thus, the scheme proposed in [25] is dependent on the operation scenarios. Second, the quasi-steady-state frequency deviation (QSSFD) under contingencies was not considered. The analysis method of frequency dynamics in [25] was only appliable to the transient process before the frequency nadir. Thus, the QSSFD can not be analyzed, and the planning scheme may fail to maintain the QSSFD within a secure range. The under-frequency load shedding (UFLS) may be activated, if the QSSFD exceeds the frequency threshold of the special stage [26], [27].

In order to address the above issues, a chance-constrained optimal configuration scheme for the BESS is proposed. First, the system frequency response (SFR) model is extended with the dynamics of the BESS, on which the required frequency regulation capability constrained by the maximum transient frequency deviation (MTFD) and QSSFD is estimated. Then, the probability density function (PDF) of the net power fluctuations of VREs and load is built by the kernel density estimation method. A multi-objective chance-constrained programming model considering the uncertainties of VREs and load, and frequency deviation is developed for the planning of the BESS. Furthermore, the optimization model is transformed into a deterministic form by the Bernstein approximation, and solved through alternating iteration.

The contributions of this paper can be summarized as follows: 1) A framework for the optimization of the BESS capacity is established to maintain both the uncertain power fluctuations and frequency deviation within predefined limits. 2) Based on the established extended system frequency response (ESFR) model, an estimation scheme of the required frequency regulation capability constrained by the MTFD and QSSFD is proposed for the BESS. 3) A multi-objective chance-constrained programming model considering the life cycle cost, energy arbitrage, uncertain power fluctuation, and frequency regulation is established to optimize the size of the BESS. 4) A solution method based on the linear weighted method, Bernstein approximation, and Benders decomposition is proposed to efficiently solve the optimization model, and obtain the size of the BESS.

The rest of this paper is organized as follows. The Section II describes the BESS planning problem. Then, the required frequency regulation capability of the BESS is estimated in Sections III. Additionally, the chance-constrained programming model is established and solved in Section IV and V, respectively. Furthermore, the case study is presented and discussed in Section VI, followed by the conclusions.

II. Problem Description

Fig. 1 shows the general structure of the power system with the BESS. The BESS is deployed with the VREs, and the local load is included. The BESS, VREs and local load are connected to the power system through the point of common coupling (PCC). The power injection into the power system can be smoothed by the BESS, which can mitigate the uncertainties of both the VREs and load. For the energy arbitrage, the BESS is able to charge more power or discharge less power at the valley of the electricity prices, and charge

This article has been accepted for publication in IEEE Transactions on Sustainable Energy. This is the author's version which has not been fully edited and content may change prior to final publication. Citation information: DOI 10.1109/TSTE.2022.3192087

less power or discharge more power at the peak. The sum of the output of the BESS, VREs, and local load is taken as the net power of the bus, and the power balance of the system is further realized by unit commitment with the consideration of the network structure and operational constraints. Besides, the net power of the bus is smoothed by the BESS to reduce the magnitude of uncertain power fluctuation and alleviate the requirement on generator ramping [28], [29].

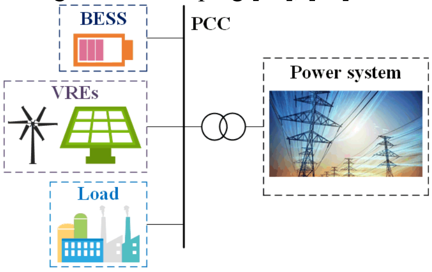

Fig. 1. General structure of power system with BESS.

Moreover, the BESS plays an important role in frequency regulation under contingencies. After a major disturbance, the BESS can coordinate with the synchronous generators to arrest frequency deviation. The VREs operate in the maximum power point tracking (MPPT) mode, and the frequency regulation service of the VREs is not considered. Fig. 2 shows the frequency dynamic response of the power system under a contingency. The system frequency first declines to a nadir and then recovers to a quasi-steady-state value. During the transient process, the primary frequency regulation (PFR) takes actions according to droop coefficients and frequency deviation. To further recover the system frequency to the nominal value, the automatic generation control (AGC) will then be activated to adjust the output of dispatchable generators. The UFLS may be activated if the MTFD exceeds the frequency threshold of the basic stage or the QSSFD exceeds the frequency threshold of the special stage [26], [27]. Therefore, the BESS is used to enhance the PFR capability to maintain the frequency deviation within secure limits.

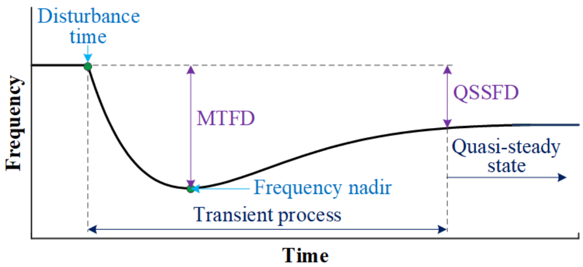

Fig. 2. Power system frequency dynamic response under a major disturbance.

As for the actual application, the proposed scheme is used to optimize the capacity of the BESS with the aim of power smoothing in normal operation, and frequency regulation under contingencies. To this end, an optimization framework accounting for the life cycle cost, uncertain power fluctuations, energy arbitrage, and frequency regulation is proposed, as illustrated in Fig. 3. First, the required frequency regulation capability of the BESS to coordinate with the synchronous generators to arrest frequency deviation under a contingency is estimated. The ESFR model is established to consider the influence of the BESS on frequency dynamic response. Based on the step-by-step summation method, the ESFR model is used to calculate the critical equivalent droop coefficient of the BESS to maintain the MTFD and QSSFD within limits. According to the critical equivalent droop coefficient, the constraints of the power capacity, power reserve and energy reserve of the BESS to ensure enough frequency regulation capability are established.

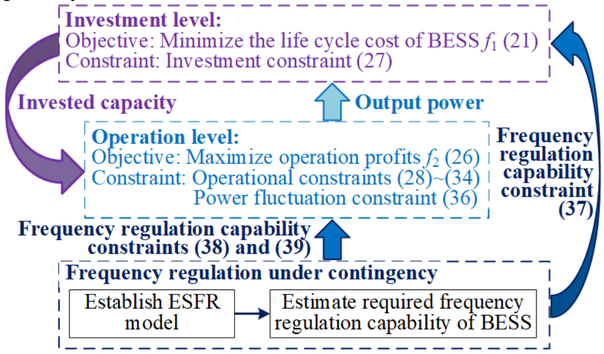

Fig. 3. Framework of proposed BESS planning scheme.

Then, in the investment level, the objective is to minimize the life cycle cost of the BESS. Besides, the constraints of the investment problem include the maximum and minimum installed capacity, and frequency regulation capability constraint on capacity. Moreover, the operation level deals with the energy arbitrage and power smoothing. With the objective of maximizing operation profits, the output of the BESS is dispatched. In the operation level, the operational constraint of the BESS, power fluctuation constraints, and frequency regulation capability constraints on power reserve and energy reserve are included.

III. Required Frequency Regulation Capability Constrained by Frequency Deviation

A. ESFR Model

The SFR model has been widely used for the analysis of frequency dynamic response under contingency. In the SFR model, the frequency of the center of inertia (COI) Δf_c is considered [30], which can be represented as,

$$\Delta f_c(s) = \frac{K_m\left(F_H + \dfrac{1-F_H}{1+T_R s}\right)\cdot \Delta P_S(s) - \Delta P_L(s)}{2Hs + D + \dfrac{K_m}{R_g}\left(F_H + \dfrac{1-F_H}{1+T_R s}\right)} \tag{1}$$

where K_m, F_H, T_R, R_g, H, and D are the gain factor, high-pressure ratio factor, reheat time constant, droop coefficient, inertia coefficient and damp coefficient, respectively. ΔP_s is the power change of AGC, and ΔP_L is the disturbance power.

The SFR model was developed with the assumption that the frequency regulation of the system is provided by synchronous generators [30]. In order to estimate the required frequency regulation capability, an ESFR model is established by integrating the influence of the BESS into the SFR model. The

This article has been accepted for publication in IEEE Transactions on Sustainable Energy. This is the author's version which has not been fully edited and content may change prior to final publication. Citation information: DOI 10.1109/TSTE.2022.3192087

BESS should inject additional power ΔP_{BESS} to arrest frequency excursion, when the power system is subject to major disturbances. The droop control is employed for the power adjustment. Besides, the system base of the SFR model is the sum of the ratings of synchronous generators [30]. The parameter of the BESS should be normalized to the system base. Thus, the operation power P_{BESS} and power change ΔP_{BESS} of the BESS can be expressed as,

$$P_{BESS}(t) = P_{BESS}(t_d) + \Delta P_{BESS}(t) \tag{2}$$

$$\Delta P_{BESS}(s) = -\frac{\Delta f_c(s)}{R_{B,e}} \cdot \frac{1}{1+T_B} \tag{3}$$

with

$$R_{B,e} = \frac{\sum_{i=1}^{n_g} S_{g,i} R_B}{S_B} \tag{4}$$

where t_d is the time of the disturbance, $R_{B,e}$ is the equivalent droop coefficient, R_B, T_B, and S_B are the droop coefficient and time constant, and power capacity of the BESS, respectively, n_g is the number of synchronous generators, and $S_{g,i}$ is the capacity of the i-th synchronous generator.

Combing (1) and (3), the ESFR model can be demonstrated in Fig. 4, of which the frequency dynamic response is represented as,

$$\Delta f_c(s) = \frac{1}{2Hs + D + \dfrac{1+F_H T_R s}{R_g(1+T_R s)} + \dfrac{1}{R_{v,e}(1+T_B s)}} \cdot \left[\Delta P_S(s) \cdot \frac{K_m + K_m F_H T_R s}{R_g(1+T_R s)} - \Delta P_L(s)\right] \tag{5}$$

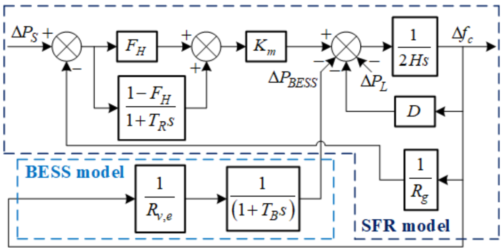

Fig. 4. Schematic diagram of proposed ESFR model.

According to Fig. 4, the synchronous generators and BESS change output based on droop coefficients, when the system is subject to disturbances. Thus, the synchronous generators and BESS take actions coordinately to arrest frequency deviation. The step response is utilized to represent the disturbances, and the AGC is not activated before frequency reaches the steady state, which can be expressed as,

$$\Delta P_L(s) = \frac{\Delta P_L}{s} \tag{6}$$

$$\Delta P_S(s) = 0 \tag{7}$$

Substituting (6) and (7) into (5) yields,

$$\Delta f_c(s) = \frac{-\Delta P_L}{2Hs^2 + Ds + \dfrac{K_m s + K_m F_H T_R s^2}{R_g(1+T_R s)} + \dfrac{s}{R_{B,e}(1+T_B s)}} \tag{8}$$

B. Frequency Regulation Capability Estimation

With regard to frequency stability control, the MTFD $\Delta f_{d,\max}$ and QSSFD Δf_s are crucial, since the UFLS may be triggered when the frequency excursion exceeds predefined thresholds. In order to improve the safety margin, the time threshold of the UFLS is not considered. Thus, the BESS is installed to coordinate with generators to make the MTFD $\Delta f_{d,\max}$ not exceed the threshold of the first stage of the UFLS, and make the QSSFD Δf_s not exceed the threshold of the special stage of the UFLS.

The estimation of equivalent parameters of the ESFR model can be represented as [30],

$$X_g = \frac{\sum_{i=1}^{n_g} X_{g,i} S_{g,i}}{\sum_{i=1}^{n_g} S_{g,i}} \tag{9}$$

where X_g and $X_{g,i}$ are the equivalent parameter and corresponding parameters of the i-th generator, respectively, and X_g and $X_{g,i}$ can be K_m, F_H, T_R, $1/R_g$, H, and D.

In order to avoid activating the UFLS, the critical equivalent droop coefficient of the BESS $R_{B,e,cri}$ can be estimated as,

$$R_{B,e,cri} = \max R_{B,e}$$
$$s.t. \begin{cases} \Delta P_L = -\Delta P_{L,\max} \\ f_N\left(1-\Delta f_{d,\max}\right) \geq f_{u,1} \\ f_N\left(1-\Delta f_s\right) \geq f_{u,s} \end{cases} \tag{10}$$

where $\Delta P_{L,\max}$ is the predefined disturbance power, f_N is the rated frequency, and $f_{u,1}$ and $f_{u,s}$ are the frequency thresholds of the first stage and special stage of the UFLS, respectively.

The step-by-step summation method can be utilized to solve the nonlinear programming (NLP) model (10) [31], and the procedures are written as Algorithm 1.

Algorithm 1: Solution method for the NLP	
Step 1:	Initialize $\Delta P_{L,\max}$, f_N, $f_{u,1}$, $f_{u,s}$, $R_{B,e}$, change step $\Delta R_{B,e}$, critical equivalent droop coefficient $R_{B,e,cri}$=0, MTFD $\Delta f_{d,\max,cri}$=0, QSSFD $\Delta f_{s,cri}$=0, and time of QSSFD $t_{s,cri}$=0.
Step 2:	Calculate $\Delta f_{d,\max}$, Δf_s and t_s by (8).
Step 3:	If f_N·(1-$\Delta f_{d,\max}$)<$f_{u,1}$ or f_N·(1-Δf_s)<$f_{u,s}$, let $R_{B,e}$=$R_{B,e}$ +$\Delta R_{B,e}$, and go back to Step 2.
Step 4:	Let $R_{B,e,cri}$=$R_{B,e}$, $\Delta f_{d,\max,cri}$=$\Delta f_{d,\max}$, $\Delta f_{s,cri}$=Δf_s, and $t_{s,cri}$=t_s, and return $R_{B,e,cri}$, $\Delta f_{d,\max,cri}$, $\Delta f_{s,cri}$, and $t_{s,cri}$.

Substituting the obtained equivalent droop coefficient $R_{B,e}$ into (4), the critical power capacity of the BESS $S_{B,cri}$ can be expressed as,

This article has been accepted for publication in IEEE Transactions on Sustainable Energy. This is the author's version which has not been fully edited and content may change prior to final publication. Citation information: DOI 10.1109/TSTE.2022.3192087

$$S_{B,cri} = \frac{\sum_{i=1}^{n_g} S_{g,i} R_B}{R_{B,e,cri}} \tag{11}$$

Moreover, the power change of the BESS increases as the frequency deviates from the nominal value. Thus, the critical power change $P_{BESS,cri}$ occurs at the frequency nadir, which can be represented as,

$$P_{BESS,cri} = \frac{\Delta f_{d,\max,cri}}{R_{B,e,cri}} \tag{12}$$

The critical energy change $E_{BESS,cri}$ is estimated according to the frequency trajectory $\Delta f_c(t)$, which can be represented as,

$$E_{BESS,cri} = \int_0^{t_{s,cri}} \frac{\Delta f_c(t)}{R_{B,e,cri}} dt + \frac{\Delta f_{s,cri}}{R_{B,e,cri}} \cdot \left(t_c - t_{s,cri}\right) \tag{13}$$

where t_c is the duration of frequency regulation of the BESS.

From (11)~(13), the required frequency regulation capability can be represented as,

$$S_{FD} = k_{r,1} S_{B,cri} \tag{14}$$

$$P_{FD} = k_{r,2} P_{BESS,cri} \tag{15}$$

$$E_{FD} = k_{r,3} E_{BESS,cri} \tag{16}$$

where S_{FD}, P_{FD} and E_{FD} are the power capacity, power reserve and energy reserve of the BESS to meet the requirement of frequency regulation, respectively, and $k_{r,1}$~$k_{r,3}$ are the ratio factors considering the influence of errors. Besides, the ratio factors $k_{r,1}$~$k_{r,3}$ are used to improve the security margin. According to the conservativeness degree of decision makers, the ratio factors can be determined by the Delphi method [32].

IV. Chance-Constrained Programming Model for BESS Planning

A. Probabilistic Model of Net Power

The net power of the VREs and local load is expressed as,

$$\begin{aligned} P_{NP,t} &= P_{VRE,t} - P_{LP,t} \\ &= P_{BNP,t} + P_{VNP,t} \end{aligned} \tag{17}$$

where $P_{NP,t}$, $P_{VRE,t}$, and $P_{LP,t}$ are the net power, VRE power, and local load at t, respectively, T is the length of the data window, $P_{BNP,t}$ is the predicted value of net power at t, and $P_{VNP,t}$ is the uncertain net power fluctuation at t.

Then, the uncertain net power fluctuation $P_{VNP,t}$ is normalized as,

$$e_{VNP,t} = \frac{P_{VNP,t}}{a_{VNP}} \tag{18}$$

with

$$a_{VNP} = \max_{t=1,\cdots,T} \left|P_{VNP,t}\right| \tag{19}$$

where $e_{VNP,t}$∈[-1, 1] is the normalized net power fluctuation at t, and a_{VNP} is an auxiliary variable.

The $\boldsymbol{e}_{VNP}$={$e_{VNP,1}$ $e_{VNP,2}$, ⋯, $e_{VNP,T}$} is the sample of T independent stochastic variables, of which the PDF f_h can be estimated by the kernel density estimation as [33],

$$f_h\left(e_{VNP}\right) = \frac{1}{Th} \sum_{t=1}^{T} K\left(\frac{e_{VNP} - e_{VNP,t}}{h}\right) \tag{20}$$

where $K(\cdot)$ is the kernel function, and h is the bandwidth.

B. Objective Function

The life cycle cost of the installed BESS is needed to be minimized. Therefore, the first optimization objective f_1 can be expressed as [34],

$$\min f_1 = C_{iv} + C_{oc} + C_{mc} + C_{dc} \tag{21}$$

with

$$C_{iv} = c_{iv} \cdot x_{BESS} \tag{22}$$

$$C_{oc} = \sum_{i=1}^{N_L} \frac{c_{oc}(1-\beta)}{(1+\alpha)^i} \cdot x_{BESS} \tag{23}$$

$$C_{mc} = \sum_{i=1}^{N_L} \frac{c_{mc}(1-\beta)}{(1+\alpha)^i} \cdot x_{BESS} \tag{24}$$

$$C_{dc} = \frac{c_{dc}(1-\beta)}{(1+\alpha)^{N_L}} \cdot x_{BESS} \tag{25}$$

where x_{BESS} as the installed number of the BESS units, respectively, and x_{BESS}∈**N**, C_{iv} is the capital cost of the BESS along with auxiliary equipment and construction work, and c_{iv} is the capital cost of the BESS unit, C_{oc}, C_{mc}, and C_{dc} are the fixed operation cost, maintenance cost, and disposal cost, respectively, c_{oc}, c_{mc}, and c_{dc} are the fixed operation cost, unit maintenance cost, and unit disposal cost of the BESS unit, respectively, α is the interest rate, β is the tax rate, and N_L is the lifespan.

In addition, the second objective is to maximize operation profits considering time-of-use electricity prices. The objective function f_2 can be represented as,

$$\begin{aligned} \max f_2 = -1 \cdot \Delta t_L \cdot \sum_{t=1}^{T_L} p_{ri,t} \cdot \Big\{ P_{BESS,c,t} \cdot \big[1+ \\ (1-\eta_{BESS,c})\big] + P_{BESS,d,t} \cdot \left[1+(1-\frac{1}{\eta_{BESS,d}})\right] \Big\} \end{aligned} \tag{26}$$

where $p_{ri,t}$ is the electricity price at t, $P_{BESS,c,t}$ and $P_{BESS,d,t}$ are the charging and discharging power of the BESS at t, respectively, $\eta_{BESS,c}$ and $\eta_{BESS,d}$ are the charging and discharging efficiencies of the BESS, respectively, Δt_L is the time step, and T_L is the operation period.

C. Constraints

1) Investment Constraint

The investment for the BESS is limited, which can be expressed as,

$$S_{BESS,\min} \le x_{BESS} S_{BESS,r} \le S_{BESS,\max} \tag{27}$$

where $S_{BESS,\max}$ and $S_{BESS,\min}$ are the maximum and minimum allowable power capacities for the BESS, respectively, and $S_{BESS,r}$ is the rated power capacity of the battery.

2) Operational Constraint

The basic constraints for the operation of the BESS can be represented as,

$$P_{BESS,c,t} \le x_{BESS} S_{BESS,r} \tag{28}$$

$$P_{BESS,c,t} \ge 0 \tag{29}$$

$$P_{BESS,d,t} \ge -x_{BESS} S_{BESS,r} \tag{30}$$

$$P_{BESS,d,t} \le 0 \tag{31}$$

$$E_{BESS,t} = E_{BESS,t-1} + \Delta t_L \cdot \left(P_{BESS,c,t} \eta_{BESS,c} + \frac{P_{BESS,d,t}}{\eta_{BESS,d}} \right) \tag{32}$$

$$x_{BESS} E_{BESS,\min} \le E_{BESS,t} \le x_{BESS} E_{BESS,\max} \tag{33}$$

$$\sum_{t=1}^{T_L} P_{BESS,c,t} \eta_{BESS,c} + \frac{P_{BESS,d,t}}{\eta_{BESS,d}} = 0 \tag{34}$$

where $E_{BESS,t}$ is the energy of the BESS at time instant t; $E_{BESS,\max}$ and $E_{BESS,\min}$ are the maximum and minimum allowable energies of the battery, respectively.

3) Power Fluctuation Constraint

The net power fluctuation of VREs and local load should be maintained within predefined limits to alleviate the requirement on generator ramping [28], [29]. With the operation of BESS, the uncertain power fluctuation of the PCC $C_{pv,t}$ is calculated by,

$$\begin{aligned} C_{pv,t} &= P_{VNP,t} - \left(P_{BESS,c,t} + P_{BESS,d,t} \right) \\ &= a_{VNP} e_{VNP,t} - \left(P_{BESS,c,t} + P_{BESS,d,t} \right) \end{aligned} \tag{35}$$

For the entire operation duration T_L, there are at least 1-γ chance that the power fluctuation should not exceed the predefined range, which can be represented as,

$$\Pr\left\{ \alpha \le C_{pv,t} \le \beta \right\} \ge 1-\gamma \tag{36}$$

where α and β are the upper and lower thresholds of net power fluctuation, respectively, and γ is the probability violation threshold, and $\gamma \in [0, 1]$.

4) Frequency Regulation Capability Constraint

In order to arrest frequency deviation under contingencies, the BESS should meet the frequency regulation capability constraint. From (14)~(16), the frequency regulation capability constraint can be represented as,

$$x_{BESS} S_{BESS,r} \ge S_{FD} \tag{37}$$

$$x_{BESS} S_{BESS,r} + P_{BESS,d,t} \ge P_{FD} \tag{38}$$

$$E_{BESS,\max} - E_{BESS,t} \ge E_{FD} \tag{39}$$

V. Solution Method for BESS Planning

The multi-objective optimization model can be transformed into a single-objective model f_m by the linear weighted method, which can be represented as,

$$\min f_m = f_1 - c_w f_2 \tag{40}$$

where c_w is the weighting coefficient. Besides, the weighting coefficient c_w measures the preference of the decision maker on the optimization objectives, and can be determined by the Delphi method [32].

In order to make the chance-constrained programming model more tractable, the Bernstein approximation is utilized to deal with the chance constraint (36). Based on the law of total probability, the conservative substitutes of (36) can be obtained and expressed as [35],

$$\Pr\left\{ C_{pv,t} \ge \alpha \right\} \ge 1 - \frac{\gamma}{2} \tag{41}$$

$$\Pr\left\{ C_{pv,t} \le \beta \right\} \ge 1 - \frac{\gamma}{2} \tag{42}$$

Then, substituting (35) in (41) and (42) yields,

$$\Pr\left\{ -a_{VNP} e_{VNP,t} + \left(P_{BESS,c,t} + P_{BESS,d,t} \right) + \alpha \le 0 \right\} \ge 1 - \frac{\gamma}{2} \tag{43}$$

$$\Pr\left\{ a_{VNP} e_{VNP,t} - \left(P_{BESS,c,t} + P_{BESS,d,t} \right) - \beta \le 0 \right\} \ge 1 - \frac{\gamma}{2} \tag{44}$$

With the use of the logarithmic moment generating function, the conservative substitutes of (43) and (44) are given by [36],

$$\begin{aligned} \inf_{v>0} \Bigg[& \left(P_{BESS,c,t} + P_{BESS,d,t} \right) + \alpha + \\ & v\Phi\left(\frac{a_{VNP}}{v} \right) + v \ln\left(\frac{2}{\gamma} \right) \Bigg] \le 0 \end{aligned} \tag{45}$$

$$\begin{aligned} \inf_{v>0} \Bigg[& -\left(P_{BESS,c,t} + P_{BESS,d,t} \right) - \beta + \\ & v\Phi\left(\frac{-a_{VNP}}{v} \right) + v \ln\left(\frac{2}{\gamma} \right) \Bigg] \le 0 \end{aligned} \tag{46}$$

with

$$\Phi(y) = \ln\left[\int \exp(yz) \mathrm{d}P_a(z) \right] \tag{47}$$

where v is the optimization variable, $\Phi(\cdot)$ is the logarithmic moment generating function, y and z are the independent variables, and P_a is the probability distribution of $e_{VRE,t}$.

Additionally, an upper-bound of the logarithmic moment generating function $\Phi(\cdot)$ can be represented as [36],

$$\Phi(x) \le \max\left\{ \mu^- x, \quad \mu^+ x \right\} + \frac{1}{2} \sigma_x^2 x^2 \tag{48}$$

where μ^-, μ^+ and σ_x are the constants that depend on the probability distribution P_a, and $-1 \le \mu^- \le \mu^+ \le 1$.

Substituting (48) in (45) and (46), and using the arithmetic-geometric inequality yields,

$$\begin{aligned} & \left(P_{BESS,c,t} + P_{BESS,d,t} \right) + \alpha + \max\left\{ -\mu^- a_{VNP}, \right. \\ & \left. -\mu^+ a_{VNP} \right\} + \frac{1}{2} \sqrt{2 \ln\left(\frac{2}{\gamma} \right)} \cdot \sqrt{\sigma_x^2 \left(-a_{VNP} \right)^2} \le 0 \end{aligned} \tag{49}$$

$$\begin{aligned} & -\left(P_{BESS,c,t} + P_{BESS,d,t} \right) - \beta + \max\left\{ \mu^- a_{VNP}, \right. \\ & \left. \mu^+ a_{VNP} \right\} + \frac{1}{2} \sqrt{2 \ln\left(\frac{2}{\gamma} \right)} \cdot \sqrt{\sigma_x^2 \left(a_{VNP} \right)^2} \le 0 \end{aligned} \tag{50}$$

The expectation μ_e and variance σ_e^2 of the net power fluctuation $e_{VRE,t}$ can be calculated by the PDF f_h as,

$$\mu_e = \int_{-1}^{1} e_{VNP} f_h\left(e_{VNP} \right) \mathrm{d}e_{VNP} \tag{51}$$

$$\sigma_e^2 = \int_{-1}^{1} \left(e_{VNP} - \mu_e \right)^2 f_h\left(e_{VNP} \right) \mathrm{d}e_{VNP} \tag{52}$$

Substituting the expectation μ_e and variance σ_e^2 in (49) and (50), the chance constraint can be transformed into a convex and deterministic form, which can be represented as,

$$\left(P_{BESS,c,t}+P_{BESS,d,t}\right)+\alpha-\mu_e a_{VNP}+\frac{1}{2}\sqrt{2\ln\left(\frac{2}{\gamma}\right)}\cdot\left|\sigma_e\right|\cdot\left|a_{VNP}\right|\le 0 \tag{53}$$

$$-\left(P_{BESS,c,t}+P_{BESS,d,t}\right)-\beta+\mu_e a_{VNP}+\frac{1}{2}\sqrt{2\ln\left(\frac{2}{\gamma}\right)}\cdot\left|\sigma_e\right|\cdot\left|a_{VNP}\right|\le 0 \tag{54}$$

Moreover, the Benders decomposition is employed to solve the obtained deterministic optimization problem, which is divided into a master problem and a subproblem. The master problem in the compact form can be represented as,

$$\min \boldsymbol{C}_1^T\boldsymbol{X}_{ins}+q$$
$$s.t.\begin{cases}\boldsymbol{A}_m\boldsymbol{X}_{ins}\le\boldsymbol{b}_m\\ \boldsymbol{X}_{ins}\in\boldsymbol{S}_o,\ \boldsymbol{X}_{ins}\in\boldsymbol{S}_f\\ q\ge 0\end{cases} \tag{55}$$

where $\boldsymbol{X}_{ins}=\{x_{BESS}\}$ is the decision variable, the first term of the objective function corresponds to the first term of (40) and $\boldsymbol{C}_1$ is the coefficient vector, q is an auxiliary variable and corresponds to the second term of (40), the first constraint includes (27) and (37), and $\boldsymbol{A}_m$ and $\boldsymbol{b}_m$ are the coefficient matrix and vector, respectively, and $\boldsymbol{S}_o$ and $\boldsymbol{S}_f$ are the sets of Benders optimality cut and feasibility cut, respectively.

In addition, the subproblem can be compactly expressed as,

$$\min \boldsymbol{C}_2^T\boldsymbol{Y}_{dis}$$
$$s.t.\begin{cases}\boldsymbol{A}_{c,1}\boldsymbol{Y}_{dis}+\boldsymbol{A}_{c,2}\boldsymbol{X}_o\le\boldsymbol{b}_c\\ \boldsymbol{A}_d\boldsymbol{Y}_{dis}\le\boldsymbol{b}_d\end{cases} \tag{56}$$

where $\boldsymbol{X}_o$ is the solution of the master problem, $\boldsymbol{Y}_{dis}=\{P_{BESS,c,t}, P_{BESS,d,t}\}$ is the decision variables, $\boldsymbol{C}_2$ is the coefficient vector and corresponds to the second term of (40), the first constraint is the coupling constraint and includes (28), (31), (33), (38) and (39), and $\boldsymbol{A}_{c,1}$, $\boldsymbol{A}_{c,2}$ and $\boldsymbol{b}_c$ are the coefficient matrices and vector, respectively, and the second constraint includes (29), (31), (32) and (34), and $\boldsymbol{A}_d$ and $\boldsymbol{b}_d$ are the coefficient matrix and vector, respectively.

The decision variable $\boldsymbol{X}_{ins}$ is the coupling variable between the master problem and subproblem. During each iteration, the master problem (55) is first solved, and the solution $\boldsymbol{X}_o$ is transferred to the subproblem (56). With the obtained solution $\boldsymbol{X}_o$, the subproblem may be feasible or infeasible. When the subproblem is feasible, a Benders optimality cut will be generated and added to the corresponding set $\boldsymbol{S}_o$. Otherwise, the set of the Benders feasibility cut $\boldsymbol{S}_f$ representing the violation of the coupling variable is expanded. A lower bound B_l can be determined by the master problem, and an upper bound B_u is calculated by the subproblem. The gap ε_g between the bounds decreases as the iteration continues. And a convergence is reached when the gap ε_g is less than a predefined tolerance ε_r. With the alternating iteration, a global optimal solution can be achieved [37]. As the iteration goes on, the feasibility region of the master problem (55) is reduced by the generated cuts. The time step of the Benders decomposition is adaptive, and determined by the obtained master problem and subproblem at each iteration [38].

Because the subproblem (56) is a linear program, the strong duality theorem can be utilized [39]. Thus, the Benders optimality cut and feasibility cut are expressed as,

$$\boldsymbol{\lambda}_{c,o}^T\left(\boldsymbol{b}_c-\boldsymbol{A}_{c,2}\boldsymbol{X}_{ins}\right)+\boldsymbol{\lambda}_{d,o}^T\boldsymbol{b}_d\le q \tag{57}$$

$$\boldsymbol{v}_c^T\left(\boldsymbol{b}_c-\boldsymbol{A}_{c,2}\boldsymbol{X}_{ins}\right)+\boldsymbol{v}_d^T\boldsymbol{b}_d\le 0 \tag{58}$$

where $\boldsymbol{\lambda}_{c,o}$ and $\boldsymbol{\lambda}_{d,o}$ are the solution vectors of the dual subproblem, and $\boldsymbol{v}_c$ and $\boldsymbol{v}_d$ are the vectors representing the unbounded ray of the dual subproblem.

The gap ε_g between the upper and lower bounds can be represented as,

$$\varepsilon_g=B_u-B_l \tag{59}$$

with

$$B_l=\max\left\{B_l,\ \boldsymbol{C}_1^T\boldsymbol{X}_o+q_o\right\} \tag{60}$$

$$B_u=\min\left\{B_u,\ \boldsymbol{C}_1^T\boldsymbol{X}_o+\boldsymbol{\lambda}_{c,o}^T\left(\boldsymbol{b}_c-\boldsymbol{A}_{c,2}\boldsymbol{X}_o\right)+\boldsymbol{\lambda}_{d,o}^T\boldsymbol{b}_d\right\} \tag{61}$$

where q_o is the solution of the master problem.

Therefore, Fig. 5 shows the optimization scheme for the BESS planning, of which the procedures are written as Algorithm 2.

Algorithm 2: Optimization scheme for the BESS planning	
Step 1:	Initialize the ESFR model (8), and estimate the required frequency regulation capability of the BESS by (14)~(16).
Step 2:	Calculate the net power by (17), preprocess the data series by (18) and (19), and estimate the PDF f_h by the kernel density estimation in (20).
Step 3:	Initialize the multi-objective chance-constrained programming model (21)~(39), and transform the model into a single-objective form by the linear weighted method in (40).
Step 4:	Utilize the Bernstein approximation to transform the chance constraint (36) into a convex and deterministic form (53) and (54).
Step 5:	Apply the Benders decomposition to the model, and divide the model into the mater problem (55) and subproblem (56).
Step 6:	Initialize ε_r, B_l=-∞, B_u=∞, $\boldsymbol{S}_o$=∅, $\boldsymbol{S}_f$=∅, and iteration number k_b=0.
Step 7:	Solve the master problem (55), transfer the solution $\boldsymbol{X}_o$ to the subproblem, let k_b=k_b+1, and update the lower bound B_l by (60).
Step 8:	If the subproblem (56) is feasible, add the Benders optimality cut (57) to the set $\boldsymbol{S}_o$. Otherwise, add the Benders feasibility cut (58) to the set $\boldsymbol{S}_f$, and go back to step 7.
Step 9:	Update the upper bound B_u by (61), and calculate the gap ε_g by (59). If $\varepsilon_g\le\varepsilon_r$, return the solution $\boldsymbol{X}_o$ and terminate. Otherwise, go back to step 7.

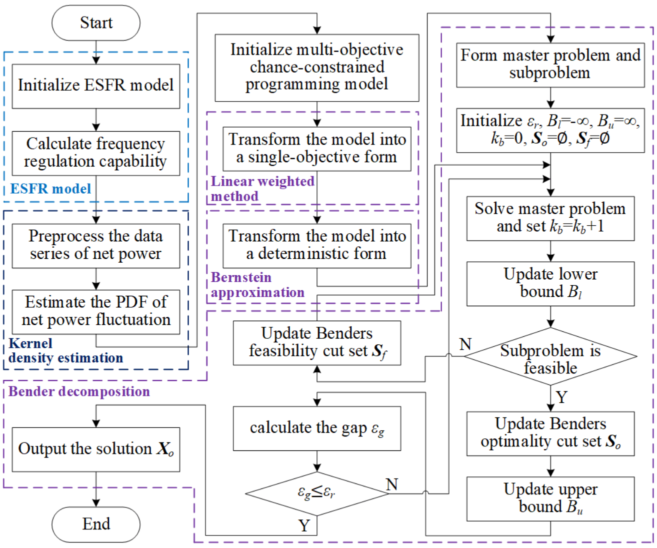

Fig. 5. Flowchart of the proposed optimization scheme for the BESS planning.

VI. Case Study

The case study was carried out on the modified IEEE 39-bus system to validate the effectiveness of the proposed scheme. Fig. 6 shows the modified IEEE 39-bus system, in which the PV station, wind farm, local load and BESS are connected to Bus 14 through the PCC. Bus 31 is the slack bus, and Generator 2 is the grid-forming unit. The capacity of the PV station and wind farm are 20 MW and 35 MW, respectively. The power output of VREs and local load of 30 typical days are demonstrated in Fig. 7, and the total time and resolution are 720 h and 1 h, respectively.

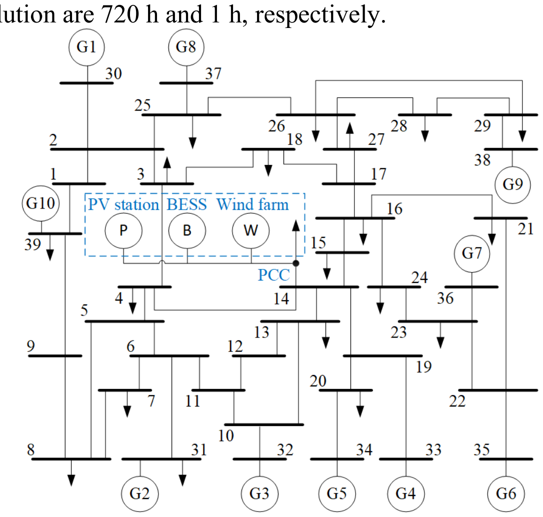

Fig. 6. Schematic diagram of modified IEEE 39-bus system.

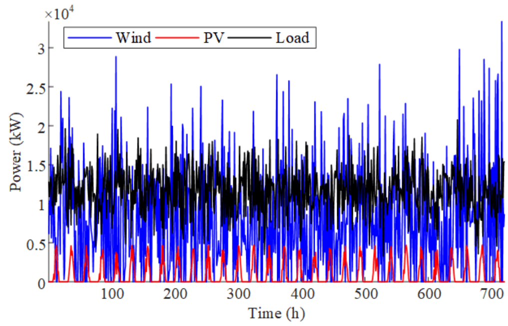

Fig. 7. Power output of VREs and local load.

Moreover, the interest rate r and tax rate β are 6% and 3%, respectively, and the lifespan N_S is 10 years. The minimum and maximum power capacities $S_{BESS,\min}$ and $S_{BESS,\max}$ for the BESS planning are 0 and 200 MW, respectively. The parameters of the BESS unit are listed in Table I. The time-of-use electricity prices $P_{ri,t}$ are listed in Table II. The time step Δt_L is 1 h, and the operation period T_L is 24 h. The power data can be divided into 30 operation scenarios. Without loss of generality, the average value of net power is taken as the predicted value.

TABLE I
PARAMETERS OF BESS UNIT

Rated power capacity $S_{BESS,r}$ (kW)	Rated energy $E_{BESS,r}$ (kW·h)	Maximum energy $E_{BESS,\max}$ (kW·h)	Minimum energy $E_{BESS,\min}$ (kW·h)
10	120	$0.9 \cdot E_{BESS,r}$	$0.2 \cdot E_{BESS,r}$
Charging efficiency $\eta_{BESS,c}$ (%)	Discharging efficiency $\eta_{BESS,d}$ (%)	Droop coefficient R_B (-)	Time coefficient T_B (s)
90	90	0.015	0.5
Capital cost c_{iv} (¥)	Maintenance cost c_{oc} (¥/ year)	Operation cost c_{mc} (¥/ year)	Disposal cost c_{dc} (¥)
400	40	30	4

TABLE II
TIME-OF-USE ELECTRICITY PRICE

Time	00:00-02:00	02:00-04:00	04:00-06:00	06:00-08:00	08:00-10:00	10:00-12:00
Electricity prices (¥/kW·h)	0.360	0.360	0.360	0.687	1.070	1.270
Time	12:00-14:00	14:00-16:00	16:00-18:00	18:00-20:00	20:00-22:00	22:00-24:00
Electricity prices (¥/kW·h)	1.170	1.070	0.687	1.170	1.070	0.687

The Power System Simulator for Engineering (PSS/E) 34.1.0 was employed for electromechanical transient simulation. The aim of the electromechanical transient simulation is to analyze the frequency dynamic response of the system under contingencies. In the simulation, the PFR from the PV station and wind farm was not considered, and the PFR was provided by the synchronous generators and BESS. For the synchronous generators, the GENROU, IEEET1, and IEEEG1 models in PSS/E were used. The electromechanical transient model of the BESS in (3) was developed on FLECS,

This article has been accepted for publication in IEEE Transactions on Sustainable Energy. This is the author's version which has not been fully edited and content may change prior to final publication. Citation information: DOI 10.1109/TSTE.2022.3192087

and compiled and converted into a user-defined model in PSS/E. The simulation time step was set as 1 ms and simulation time was set as 15 s. The rated system frequency f_N is 60 Hz, and the thresholds of the first stage and special stage $f_{u,1}$ and $f_{u,s}$ of the UFLS are 59.2 Hz and 59.6 Hz, respectively. The maximum disturbance power $\Delta P_{L,\max}$ is set as -0.15 p.u., and the change step $\Delta R_{B,e}$ is set as -0.001. The duration of transient frequency regulation t_c is set as 30 s, and the ratio factors $k_{r,1}$~$k_{r,3}$ are set as 1.02.

The Gaussian kernel function is utilized to estimate the PFD of net power fluctuations f_h, and the bandwidth h is set as 0.084. The lower threshold α and upper threshold β of net power fluctuations are set as -20 MW and 20 MW, respectively. The probability violation threshold γ are set as 10%. Additionally, the weighting coefficient c_w sis set as 1000, and the convenience tolerance ε_r is set as 0.0001.

A. Optimization Results of BESS Planning

The PDF f_h of the normalized net power fluctuation can be demonstrated in Fig. 8. The optimized number of the BESS units x_{BESS} is 18,180, and the power capacity S_B is 181.8 MW. In addition, the values of the objective function f_m, f_1, and f_2 are -1.2724×10^7, 1.6397×10^7, and 2.9121×10^4, respectively. The life cycle cost of the installed BESS is 1.6397×10^7 ¥, and the operation profits of an operation period T_L is 2.9121×10^4 ¥.

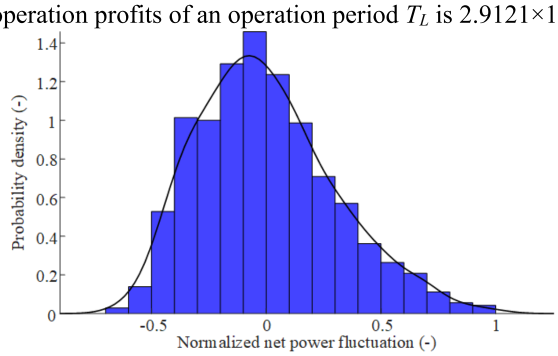

Fig. 8. Probability density curve of normalized net power fluctuation.

When the system is subject to the maximum disturbance power $\Delta P_{L,\max}$, the MTFD and QSSFD are -0.764 Hz and -0.398 Hz, respectively. In addition, the frequency nadir and quasi-steady-state frequency are 59.236 Hz and 59.602 Hz, respectively. The UFLS is not activated, which verifies the effectiveness of the proposed scheme to arrest frequency deviation under contingency. Moreover, the operation power of the BESS and the power fluctuation of the PCC $C_{pv,t}$ are demonstrated in Fig. 9. The probability that the power fluctuation $C_{pv,t}$ exceeds the predefined range [α, β] is 9.86 % and less than the probability violation threshold γ. The results show that the proposed scheme is effective for power smoothing while performing energy arbitrage.

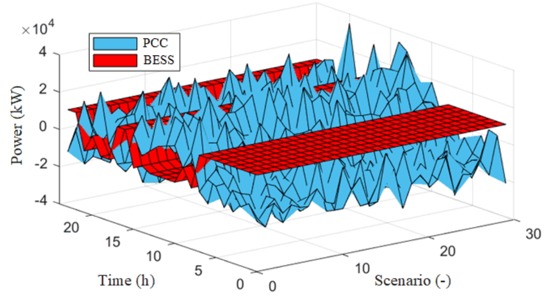

Fig. 9. Curve of BESS power and PCC power fluctuation.

B. Performance Analysis in Normal Operation

In the normal operating state, the BESS is to smooth local power fluctuation. To analyze the performance of the proposed scheme for power smoothing, the following schemes are utilized for comparison.

Scheme 1: The scheme where the constraints of power fluctuation in (36) and frequency regulation capability in (37) ~(39) were not considered.

Scheme 2: The scheme proposed in [25], where the first 20 operation scenarios were used, and the net power fluctuation was also maintained in [-20 MW, 20 MW].

According to the obtained PDF f_h, the Monte Carlo method is utilized to generate 100 operation scenarios, as shown in Fig. 10. Then, the performances of the proposed scheme, Scheme 1, and Scheme 2 are analyzed by the generated operation scenarios. According to the operation period T_L of the BESS, the sample size is 2400. The power curves of different schemes are demonstrated in Figs. 11~13. Correspondingly, the probability that the power fluctuation $C_{pv,t}$ exceeds the predefined range is summarized in Table III.

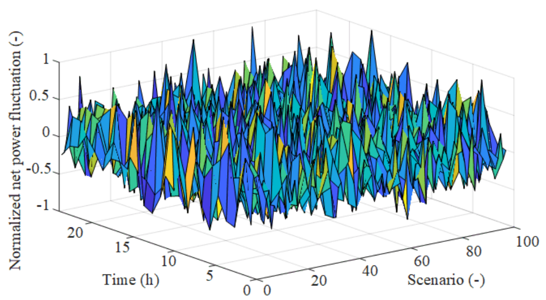

Fig. 10. Generated data of normalized net power fluctuation.

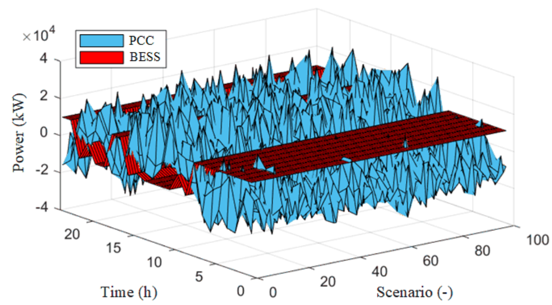

Fig. 11. Power curve of proposed scheme.

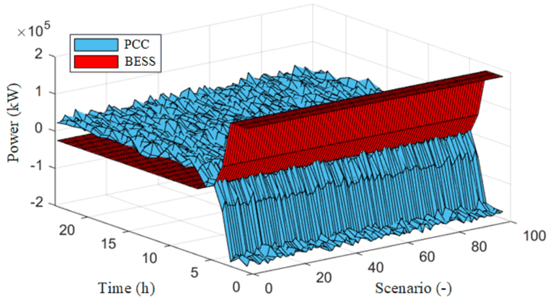

Fig. 12. Power curve of Scheme 1.

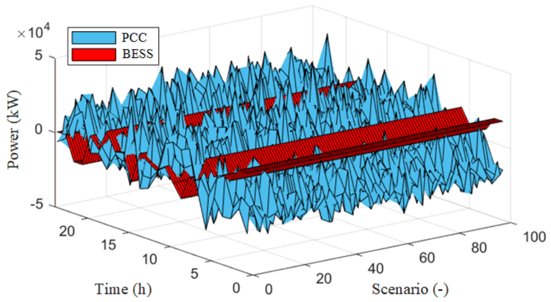

Fig. 13. Power curve of Scheme 2.

TABLE III
VIOLATION NUMBERS AND PROBABILITIES OF DIFFERENT SCHEMES

Scheme	Proposed scheme	Scheme 1	Scheme 2
Violation number (-)	233	1789	277
Violation probability (%)	9.71	76.54	11.54

It is clear that the proposed scheme is effective to maintain the violations within the threshold γ, of which the probability is 9.71%. The violation probability of Scheme 1 is 76.54%, which shows severe power fluctuation of the PCC. In addition, Scheme 2 is able to decrease the number of violations but fails to maintain the probability within the threshold γ. The results demonstrate that the proposed scheme outperforms the comparative schemes in regard to maintaining the violations within the threshold.

C. Performance Analysis under Contingency

When the system is subject to a major disturbance, the BESS is used to enhance the PFR capability of the system to arrest frequency deviation. The performance of the proposed scheme under contingencies is analyzed. Additionally, the sudden load increase and generation outage are considered in the disturbance scenarios [30]. The snapshot of the system at 10:00 in the first scenario in Fig. 10 is taken as the pre-contingency state. For comparisons, the following schemes are added.

Scheme 3: The scheme where the constraints of frequency regulation capacity on the power reserve and energy reserve of the BESS in (38) and (39) were not considered.

Scheme 4: The scheme where the constraint of frequency regulation capacity on the energy reserve of the BESS in (39) was not considered.

Disturbance 1 is set to occur at 2.0 s. The load at Bus 6 increases by 1,105 MW/1.5 p.u. suddenly, which corresponds to the maximum disturbance power $\Delta P_{L,\max}$. The frequency dynamic response of COI is shown in Fig. 14. The MTFD and QSSFD of the proposed scheme are maintained within the predefined ranges where the first stage and special stage of the UFLS are not activated. In contrast, the MTFDs of the Schemes 1, 3, and 4 exceed the threshold of the first stage of UFLS. The QSSFDs of the Schemes 1~4 exceed the threshold of the special stage of UFLS. The frequency dynamic response characteristics of the system under Disturbance 1 are summarized in Table IV. The results show that the proposed scheme has superior performance in arresting the frequency deviation and preventing the actuation of the UFLS.

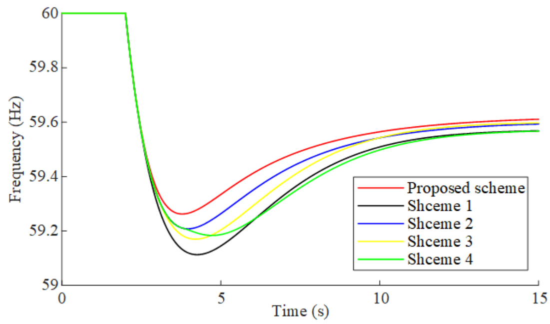

Fig. 14. Frequency dynamic response under Disturbance 1.

TABLE IV
FREQUENCY DYNAMIC RESPONSE CHARACTERISTICS UNDER DISTURBANCE 1

Scheme	Proposed scheme	Scheme 1	Scheme 2	Scheme 3	Scheme 4
MTFD (Hz)	-0.738	-0.887	-0.792	-0.830	-0.816
QSSFD (Hz)	-0.389	-0.432	-0.407	-0.403	-0.433
Frequency nadir (Hz)	59.262	59.113	59.208	59.170	59.184
Quasi-steady-state frequency (Hz)	59.611	59.568	59.593	59.597	59.597

Disturbance 2 is set to occur at 2.0 s, when the generator G10 is tripped suddenly. The generator G10 has the largest capacity, and the disturbance power is -1,000 MW/-1.357 p.u.. The frequency dynamic response of COI is shown in Fig. 15. Additionally, the frequency dynamic response characteristics under Disturbance 2 are listed in Table V. Although the power deficit caused by Disturbance 2 is smaller than Disturbance 1, the number of online generators decreases, and so the frequency regulation capability and inertia of the system is reduced. Thus, Disturbance 2 appears to be as severe as Disturbance 1. It is obvious that the MTFD and QSSFD of the proposed scheme do not exceed the frequency threshold of the UFLS. The comparative schemes fail to maintain the frequency deviation within the predefined range. The results demonstrate that the proposed scheme has superior performance in reducing frequency deviation, and is effective under both the demand- and supply-side disturbances.

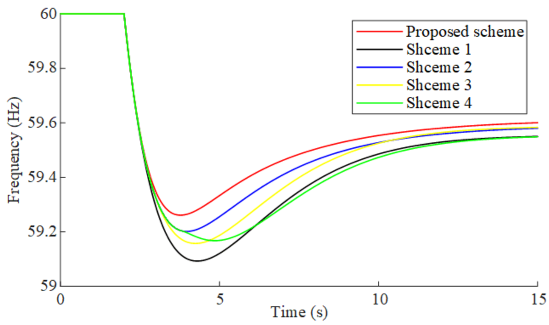

Fig. 15. Frequency dynamic response under Disturbance 2.

TABLE V
FREQUENCY DYNAMIC RESPONSE CHARACTERISTICS UNDER DISTURBANCE 2

Scheme	Proposed scheme	Scheme 1	Scheme 2	Scheme 3	Scheme 4
MTFD (Hz)	-0.739	-0.907	-0.799	-0.843	-0.832
QSSFD (Hz)	-0.399	-0.450	-0.420	-0.417	-0.451
Frequency nadir (Hz)	59.261	59.093	59.201	59.157	59.168
Quasi-steady-state frequency (Hz)	59.601	59.550	59.580	59.583	59.549

D. Sensitivity Analysis and Computational Performance

The PFR capability and equivalent inertia have great influence on the system frequency dynamic response of the system, and the required frequency regulation capability of the BESS. Therefore, the influence of the droop coefficients R_g and inertia coefficient H in (5) on the optimization result is analyzed. The values of $1/R_g$ and H are set to increase from their 80% to 120% with the step size of 5%. The corresponding change of the optimized number of the BESS units x_{BESS} is shown in Fig. 16.

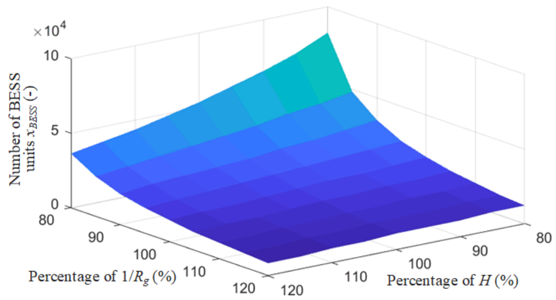

Fig. 16. Influence of droop coefficient and inertia coefficient on optimization result.

According to Fig. 16, the required frequency regulation capability of the BESS and the optimized number of the BESS units x_{BESS} decrease as $1/R_g$ and H increase. The increase of $1/R_g$ represents the enhancement of the PFR capability of the system. Additionally, the inertia coefficient H measures the equivalent inertia of the system to counter active power disturbances. Therefore, the required frequency regulation capability of the BESS and the optimization result decrease with the increase of $1/R_g$ and H.

As $1/R_g$ and H increase, the decrease of the number of the BESS units x_{BESS} is accelerated. It is clear that the droop coefficient R_g has more influence on the optimization result. The results show that the PFR capability and equivalent inertia of the system should be maintained within a reasonable range. It is inacceptable to use the BESS as the only solution to handle the frequency deviation problem under contingencies. Although the optimization result is influenced by the system parameters, the ratio factors $k_{r,1}$~$k_{r,3}$ are used to improve the security margin.

The proposed chance-constrained programming model is solved by the Bernstein approximation and Benders decomposition. In order to analyze the computational performance of the solution method, the following schemes are utilized for comparison.

Scheme 5: The scheme where the chance-constrained programming model is solved by the Monte Carlo method and particle swarm optimization (PSO) algorithm [40]. The convenience tolerance was also set as 0.0001, and the number of particles was set as 50.

Scheme 6: The scheme where the chance-constrained programming model is solved by the two-point estimation method and PSO algorithm [41]. The convenience tolerance was also set as 0.0001, and the number of particles was also set as 50.

The solution methods were implemented on MATLAB R2019b, and tested on a laptop with a 2.8-GHz Intel Core i7-1165G7 processor and 16-GB memory. The calculation process is performed 100 times, and the mean values of the iteration number and solution are listed in Table VI. It is clear that the proposed solution method can efficiently solve the established model. Compared to Schemes 5 and 6, the proposed solution method has superior performance in reducing the iteration number and solution time.

TABLE VI
COMPUTATIONAL PERFORMANCE ANALYSIS

Scheme	Proposed scheme	Scheme 5	Scheme 6
Iteration number (-)	9	47	31
Solution time (s)	72.3	694.5	443.1

VII. CONCLUSION

The paper proposes a chance-constrained optimal planning scheme for the BESS considering the uncertainties of VREs and load, and frequency regulation capability under contingencies. The required frequency regulation capability of the BESS constrained by the MTFD and QSSFD is estimated through a developed ESFR model and the step-by-step summation method. The kernel density estimation is utilized to obtain the PDF of the stochastic fluctuations of VREs and load. A multi-objective chance-constrained programming model accounting for the life cycle cost, energy arbitrage, uncertain power fluctuation, MTFD, and QSSFD is established. Based on the linear weighted method, Bernstein approximation, and Benders decomposition, the optimization model is solved to obtain the size of the BESS.

The case study results show the superior performance of the proposed scheme in smoothing net power fluctuations and reducing frequency deviation. The proposed scheme is effective to maintain the stochastic power fluctuation within the predefined bounds while performing energy arbitrage. Additionally, the proposed scheme is effective to arrest frequency excursion without activating the UFLS under both the demand- and supply-side disturbances.

In the future work, the post-contingency line overload will be taken into account, and the planning scheme of the BESS to arrest frequency deviation and alleviate post-contingency line overload will be presented.

REFERENCES

[1] H. Li, Z. Lu, Y. Qiao, *et al*., "The flexibility test system for studies of variable renewable energy resources," *IEEE Trans. Power Syst.*, vol. 36, no. 2, pp. 1526-1536, 2020.

[2] Z. Zhuo, N. Zhang, J. Yang, *et al*., "Transmission expansion planning test system for AC/DC hybrid grid with high variable renewable energy penetration," *IEEE Trans. Power Syst.*, vol. 35, no. 4, pp. 2597-2608, 2019.

[3] Y. Cao, Y. Zhang, H. Zhang, *et al*., "Probabilistic optimal PV capacity planning for wind farm expansion based on NASA data," *IEEE Trans. Power Syst.*, vol. 8, no. 3, pp. 1291-1300, 2017.

[4] C. Phurailatpam, Z. H. Rather, B. Bahrani, *et al*., "Measurement-based estimation of inertia in AC microgrids," *IEEE Trans. Sustain. Energy*, vol. 11, no. 3, pp. 1975-1984, 2019.

[5] C. A. Agostini, F. A. Armijo, C. Silva, *et al*., "The role of frequency regulation remuneration schemes in an energy matrix with high penetration of renewable energy," *Renew. Energ.*, vol. 171, pp. 1097-1114, 2021.

[6] H. Saber, H. Heidarabadi, M. Moeini-Aghtaie, *et al*., "Expansion planning studies of independent-locally operated battery energy storage systems (BESSs): a CVaR-based study," *IEEE Trans. Sustain. Energy*, vol. 11, no. 4, pp. 2109-2118, 2019.

[7] G. Pulazza, N. Zhang, C. Kang, *et al*., "Transmission planning with battery-based energy storage transportation for power systems with high penetration of renewable energy," *IEEE Trans. Power Syst.*, vol. 36, no. 6, pp. 4928-4940, 2021.

[8] B. Wang, C. Zhang, C. Li, *et al*., "Hybrid interval-robust adaptive battery energy storage system dispatch with SoC interval management for unbalanced microgrids," *IEEE Trans. Sustain. Energy*, vol. 13, no. 1, pp. 44-55, 2022.

[9] Z. Guo, W. Wei, L. Chen, *et al*., "Economic value of energy storages in unit commitment with renewables and its implication on storage sizing," *IEEE Trans. Sustain. Energy*, vol. 12, no. 4, pp. 2219-2229, 2021.

[10] I. Alsaidan, A. Khodaei, W. Gao. "A comprehensive battery energy storage optimal sizing model for microgrid applications," *IEEE Trans. Power Syst.*, vol. 33, no. 4, pp. 3968-3980, 2017.

[11] T. Sayfutdinov, C. Patsios, P. Vorobev, *et al*., "Degradation and operation-aware framework for the optimal siting, sizing, and technology selection of battery storage," *IEEE Trans. Sustain. Energy*, vol. 11, no. 4, pp. 2130-2140, 2019.

[12] X. Jiang, Y. Jin, X. Zheng, *et al*., "Optimal configuration of grid-side battery energy storage system under power marketization," *Appl. Energy*, vol. 272, pp. 115242, 2020.

[13] T. Wan, Y. Tao, J. Qiu, *et al*., "Data-driven Hierarchical Optimal Allocation of Battery Energy Storage System," *IEEE Trans. Sustain. Energy*, vol. 12, no. 4, pp. 2097-2109, 2021.

[14] A. Ehsan, Q. Yang. "Coordinated investment planning of distributed multi-type stochastic generation and battery storage in active distribution networks," *IEEE Trans. Sustain. Energy*, vol. 10, no. 4, pp. 1813-1822, 2018.

[15] S. Zhong, J. Qiu, L. Sun, *et al*., "Coordinated planning of distributed WT, shared BESS and individual VESS using a two-stage approach," *Int. J. Elec. Power Energy Syst.*, vol. 114, pp. 105380, 2020.

[16] R. Khezri, A. Mahmoudi, M. H. Haque. "A demand side management approach for optimal sizing of standalone renewable-battery systems," *IEEE Trans. Sustain. Energy*, vol. 12, no. 4, pp. 2184-2194, 2021.

[17] P. H. Divshali, C. Evens. "Optimum operation of battery storage system in frequency containment reserves markets," *IEEE Trans. Smart Grid*, vol. 11, no. 6, pp. 4906-4915, 2020.

[18] X. Wang, L. Ying, K. Wen, *et al*., "Bi-level non-convex joint optimization model of energy storage in energy and primary frequency regulation markets," *Int. J. Elec. Power Energy Syst.*, vol. 134, pp. 107408, 2022.

[19] F. Conte, S. Massucco, G. P. Schiapparelli, *et al*., "Day-ahead and intra-day planning of integrated BESS-PV systems providing frequency regulation," *IEEE Trans. Sustain. Energy*, vol. 11, no. 3, pp. 1797-1806, 2019.

[20] U. Datta, A. Kalam, J. Shi. "Battery energy storage system to stabilize transient voltage and frequency and enhance power export capability," *IEEE Trans. Power Syst.*, vol. 34, no. 3, pp. 1845-1857, 2018.

[21] W. Xing, H. Wang, L. Lu, *et al*., "An adaptive virtual inertia control strategy for distributed battery energy storage system in microgrids," *Energy*, vol. 233, pp. 121155, 2021.

[22] T. Zhao, A. Parisio, J. V. Milanović. "Distributed control of battery energy storage systems for improved frequency regulation," *IEEE Trans. Power Syst.*, vol. 35, no. 5, pp. 3729-3738, 2020.

[23] J. Cao, W. Du, H. Wang, *et al.*, "Optimal sizing and control strategies for hybrid storage system as limited by grid frequency deviations." *IEEE Trans. Power Syst.*, vol. 33, no. 5, pp. 5486-5495, 2018.

[24] S. Yan, Y. Zheng, D. J. Hill. "Frequency constrained optimal siting and sizing of energy storage," *IEEE Access*, vol. 7, pp. 91785-91798, 2019.

[25] Y. Cao, Q. Wu, H. Zhang, *et al.*, "Optimal sizing of hybrid energy storage system considering power smoothing and transient frequency regulation," *Int. J. Electr. Power Energy Syst.*, vol. 142, pp. 108227, 2022.

[26] H. Liu, H. Pan, N. Wang, *et al.*, "Robust under-frequency load shedding with electric vehicles under wind power and commute uncertainties," *IEEE Trans. Smart Grid*, doi: 10.1109/TSG.2022.3172726.

[27] *IEEE Guide for the Application of Protective Relays Used for Abnormal Frequency Load Shedding and Restoration*, IEEE Standard C37.117-2007, Aug. 2007.

[28] M. Yang, L. Zhang, Y. Cui, *et al.*, "Investigating the wind power smoothing effect using set pair analysis," *IEEE Trans. Sustain. Energy*, vol. 11, no. 3, pp. 1161-1172, 2019.

[29] S. Patel, M. Ahmed, S. Kamalasadan. "A novel energy storage-based net-load smoothing and shifting architecture for high amount of photovoltaics integrated power distribution system," *IEEE Trans. Ind. Appl.*, vol. 56, no. 3, pp. 3090-3099, 2020.

[30] Y. Cao, H. Zhang, Y. Zhang, *et al.*, "Extending SFR model to incorporate the influence of thermal states on primary frequency response," *IET Gener. Transm. Dis.*, vol. 14, no. 19, pp. 4069-4078, 2020.

[31] F. Shi, H. Zhang, Y. Cao, *et al.*, "Enhancing event-driven load shedding by corrective switching with transient security and overload constraints," *IEEE Access*, vol. 7, pp. 101355-101365, 2019.

[32] X. Xu, Y. Cao, H. Zhang, *et al.*, "A multi-objective optimization approach for corrective switching of transmission systems in emergency scenarios," *Energies*, vol. 10, no. 8, pp. 1204, 2017.

[33] B. Khorramdel, C. Y. Chung, N. Safari, *et al.*, "A fuzzy adaptive probabilistic wind power prediction framework using diffusion kernel density estimators," *IEEE Trans. Power Syst.*, vol. 33, no. 6, pp. 7109-7121, 2018.

[34] Y. Zheng, Y. Song, A. Huang, *et al.*, "Hierarchical optimal allocation of battery energy storage systems for multiple services in distribution systems," *IEEE Trans. Sustain. Energy*, vol. 11, no. 3, pp. 1911-1921, 2019.

[35] N. Y. Soltani, A. Nasiri. "Chance-constrained optimization of energy storage capacity for microgrids," *IEEE Trans. Smart Grid*, vol. 11, no. 4, pp. 2760-2770, 2020.

[36] A. Ben-Tal, L. E. Ghaoui, A. Nemirovski. *Robust optimization*, New Jersey, USA: Princeton University Press, 2009.

[37] C. Lin, W. Wu, B. Zhang, *et al.*, "Decentralized solution for combined heat and power dispatch through benders decomposition," *IEEE Trans. Sustain. Energy*, vol. 8, no. 4, pp. 1361-1372, 2017.

[38] M. Vahedipour-Dahraie, H. Rashidizadeh-Kermani, A. Anvari-Moghaddam, *et al.*, "Flexible stochastic scheduling of microgrids with islanding operations complemented by optimal offering strategies," *CSEE J. Power Energy Syst.*, vol. 6, no. 4, pp. 867-877, 2020.
[39] S. Boyd, S. P. Boyd, L. Vandenberghe L. *Convex optimization*, Cambridge, England: Cambridge University Press, 2004.
[40] J. Wu, J. Zhu, G. Chen, *et al.*, "A hybrid method for optimal scheduling of short-term electric power generation of cascaded hydroelectric plants based on particle swarm optimization and chance-constrained programming," *IEEE Trans. power syst.*, vol. 23, no. 4, pp. 1570-1579, 2008.
[41] Y. Huang, L. Wang, W. Guo, *et al.*, "Chance constrained optimization in a home energy management system," *IEEE Trans. Smart Grid*, vol. 9, no. 1, pp. 252-260, 2018.

Yongji Cao (Member, IEEE) received the B.E. and Ph.D. degrees in electrical engineering from Shandong University, Jinan, China, in 2016 and 2020, respectively. He was a Research Assistant with the School of Electrical Engineering, Shandong University, Jinan, China, from January 2021 to September 2021. He is currently a Postdoctoral Researcher with the Department of Electrical Engineering, Technical University of Denmark, Kgs. Lyngby, Denmark. His research interests include power system frequency stability analysis and control, renewable energy integration, and application of energy storage technology.

Qiuwei Wu (Senior Member, IEEE) obtained the PhD degree in Power System Engineering from Nanyang Technological University, Singapore, in 2009. He has been a tenured Associate Professor with Tsinghua-Berkeley Shenzhen Institute, Tsinghua Shenzhen International Graduate School, Tsinghua University since Jan. 2022. He was a senior R&D engineer with Vestas Technology R&D Singapore Pte Ltd from Mar. 2008 to Oct. 2009. He was working at Department of Electrical Engineering, Technical University of Denmark (DTU) from Nov. 2009 to Aug. 2021 (PostDoc Nov. 2009-Oct. 2010, Assistant Professor Nov. 2010-Aug. 2013, Associate Professor Sept. 2013-Aug. 2021).

His research interests are decentralized/distributed optimal operation and control of power and energy systems with high penetration of renewables, including distributed wind power modelling and control, decentralized/distributed congestion management, voltage control and load restoration of active distribution networks, and decentralized/distributed optimal operation of integrated energy systems.

Hengxu Zhang (Member, IEEE) received his B.E. degree in electrical engineering from Shandong University of Technology, in 1998, and his M.S. and Ph.D. in electrical engineering from Shandong University, in 2000 and 2003, respectively. He is now a professor with the Key Laboratory of Power System Intelligent Dispatch and Control of Ministry of Education (Shandong University), P. R. China. His main research interests include power system security and stability assessment, power system monitoring, and numerical simulation.

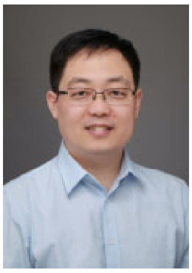

Changgang Li (Member, IEEE) received the B.E. and Ph.D. degrees in electrical engineering from Shandong University, Jinan, China, in 2006 and 2012, respectively. He was a Research Scholar with the School of Electrical Engineering and Computer Science, the University of Tennessee, Knoxville, from 2012 to 2014. He is currently a Professor with the School of Electrical Engineering, Shandong University, China. His research interests include power system operation and control.

Xuan Zhang (Senior Member, IEEE) received the B.Eng. degree in Automation from Tsinghua University in 2011, and the Ph.D. degree in Control and Electrical Engineering from the University of Oxford in 2015. From 2015 to 2018, he was a Post-Doctoral Fellow with the School of Engineering and Applied Sciences and the Harvard Center for Green Buildings and Cities, Harvard University. Since March 2018, he has been with the Tsinghua-Berkeley Shenzhen Institute, Tsinghua Shenzhen International Graduate School, Tsinghua University, where he is currently an Assistant Professor with the Smart Grid and Renewable Energy Laboratory. His current research interests include the control and optimization for cyber-physical systems (such as smart grids, smart buildings, and energy Internet), control system structure (re)design, and learning-based control. He is the recipient of Best Conference Paper in 2019 and 2021 IEEE Power & Energy Society General Meeting.